Dynamics of clusters: From elementary to biological structures

Po-Yuan Cheng[†], J. Spencer Baskin, and Ahmed H. Zewail[§]

Laboratory for Molecular Sciences, Arthur Amos Noyes Laboratory of Chemical Physics, California Institute of Technology, Pasadena, CA 91125

Edited by A. Welford Castleman, Jr., Pennsylvania State University, University Park, PA, and approved January 6, 2006 (received for review August 16, 2005)

Between isolated atoms or molecules and bulk materials there lies a class of unique structures, known as clusters, that consist of a few to hundreds of atoms or molecules. Within this range of ''nanophase,'' many physical and chemical properties of the materials evolve as a function of cluster size, and materials may exhibit novel properties due to quantum confinement effects. Understanding these phenomena is in its own rights fundamental, but clusters have the additional advantage of being controllable model systems for unraveling the complexity of condensed-phase and biological structures, not to mention their vanguard role in defining nanoscience and nanotechnology. Over the last two decades, much progress has been made, and this short overview highlights our own involvement in developing cluster dynamics, from the first experiments on elementary systems to model systems in the condensed phase, and on to biological structures.

In the early 1980s, our research group at Caltech began exploring real-time dynamics of clusters (1–5) by studying time-resolved spectroscopy, with picosecond (ps) and then femtosecond (fs) resolution (6–8), in molecular jets and beams (9, 10). These first results (ref. 11; for commentary, see ref. 12) opened the door for many more applications as they clearly elucidated in real time the influence of microsolvation and stepwise solvation effects on reactivity and photophysical processes in clusters (12). The ultimate goal we had in mind was to "bridge" the gap between the isolated-molecule behavior and that in the bulk phase, and to understand at a microscopic level the influence of solvent on reactions.

The scope of phenomena studied varied, from the influence of one-atom solvation and caging (13–19), to stepwise solvation of acid-base (20–22) and isomerization reactions (23, 24) in clusters of up to 30 solvent molecules. Both electron (25–28) and proton transfer (20–22, 29) processes were also studied, elucidating for the former one of the classics for Mulliken's dative bonded complexes, that of benzene-iodine, and for the latter the dynamics of single and double proton transfer. With mass selection, we investigated ionic clusters, the premier being solvated electrons (30) and dioxygen anions (31–33); both are important in biological activities. For chemical reactions, we used this approach of complexation to study bimolecular reactive (34–37) and nonreactive (38) scattering, and, by analogy, biomolecular structures exhibiting dative bonding and involved in molecular recognition (39–41). A descriptive outline of the work over two decades is given in Fig. 1, including relevant references (refs. 6–8 and 13–49; ref. 50 and references therein). In what follows, we only highlight some prototypical examples.

Bimolecular Reactions

Early in the development of fs transition-state spectroscopy (51) it was possible to directly probe the transition state by real-time clocking of a unimolecular reaction (half collision): $ABC^* \rightarrow A\cdots B\cdots C^{*\ddagger} \rightarrow AB + C$. For a bimolecular reaction, the full collision must be considered:

$$A + BC \rightarrow A\cdots B\cdots C^{\ddagger} \rightarrow AB + C \text{ (bimolecular).}$$

Crossed-molecular-beam techniques have been used to indirectly infer the lifetime of the collision complex from measured product angular distributions. However, for real-time clocking, the zero-of-time needs to be defined. This difficulty was addressed by initiating the reaction in a van der Waals (vdW) complex, an approach introduced for studies of product-state distributions by Soep and Wittig (see ref. 52 and references therein). In such bimolecular complexes, the two reactants are held together by a weak vdW force in a relatively well defined geometry. The reaction is initiated by an ultrashort pulse that induces a direct ejection of a radical with a given translational energy to react with another reactant. The total collision energy can be varied by tuning the laser pulse or by changing the counter fragment of the precursor. Naturally, the reaction starts from a vdW geometry and not from all impact-encounter geometries, and some energy and geometry corrections need to be considered for comparison with full-collision experiments (52).

Using this approach, we first carried out real-time clocking of the following abstraction reaction (34, 35).

$$H + CO_2 \rightarrow HOCO^{\ddagger} \rightarrow CO + OH \text{ (abstraction)}$$

The reaction was initiated in the precursor complex $IH\cdots CO_2$ by breaking the H–I bond with an ultrafast pulse; a second delayed pulse then probed the OH product by using laser-induced fluorescence. The decay of $HOCO^{\ddagger}$ was observed in the buildup of the OH final product. The results showed that the reaction's collision complex has a relatively long lifetime, about a ps. Wittig's group, with sub-ps resolution, obtained the lifetime as a function of energy, from 0.25 ps to 1.6 ps depending on total collision energy (52, 53).

Other systems studied in this group are those of halogen-exchange reactions (36, 37, 52):

$$Br + I_2 \rightarrow Br\cdots I\cdots I^{\ddagger} \rightarrow BrI + I \text{ (exchange).}$$

The reaction was initiated in an $HBr\cdots I_2$ complex by breaking the H–Br bond. The dynamics was resolved on the fs to ps time scale by detecting the BrI product. In this case, the H–Br bond is broken in fs, and the hydrogen atom flies away from the field of the reaction, eliminating complication from a third body. The rise time of the BrI product build-up was found to be 53 ps; it was 44 ps for $DBr\cdots I_2$, for which the collision energy is higher. Unlike $H + CO_2$ abstraction, the reaction goes through a "sticky long-lived collision complex." Such lifetimes of intermediates cannot be obtained by using "rotational clock-

Conflict of interest statement: No conflicts declared.

This paper was submitted directly (Track II) to the PNAS office.

[†]Permanent address: Department of Chemistry, National Tsing Hua University, Hsinchu 300, Taiwan.

[§]To whom correspondence should be addressed. E-mail: zewail@caltech.edu.

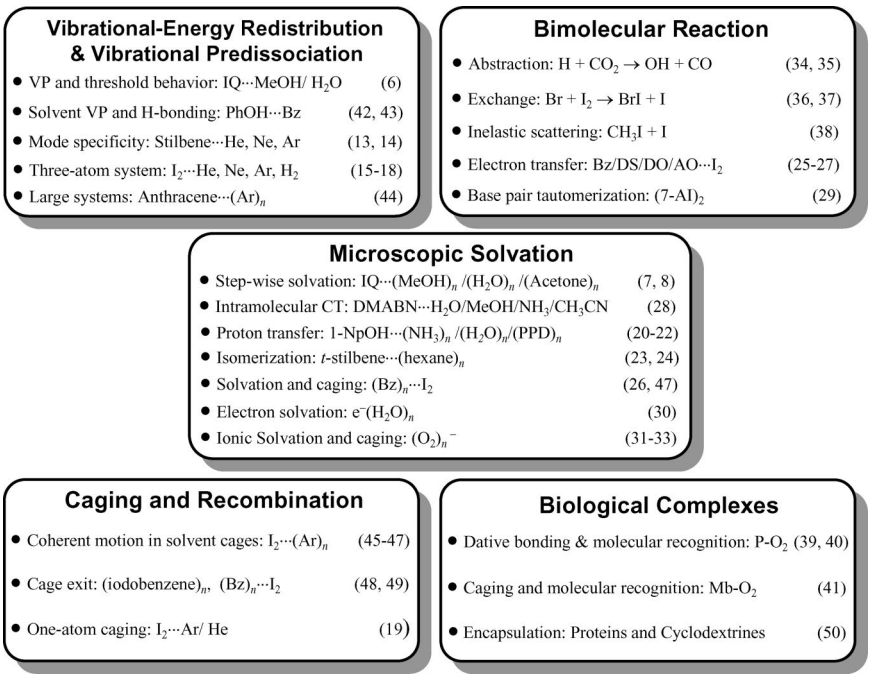

Fig. 1. An overview of major subjects and systems studied since 1983. References are given in parentheses. VP, vibrational predissociation; CT, charge transfer; IQ, isoquinoline; PhOH, phenol; Bz, benzene; DS, diethyl sulfide; DO, *p*-dioxane; AO, acetone; MeOH, methanol; DMABN, *p*-(dimethylamino) benzonitrile; AI, azaindole; NpOH, 1-naphthol; PPD, piperidine; P, picket-fence cobalt(II) porphyrin; Mb, myoglobin.

ing'' in crossed molecular beam studies. Classical trajectory calculations were carried out on a qualitative Br–I–I potential energy surface, and the results support the stability of a BrII intermediate ''molecule'' (37). McDonald's group studied the same system and obtained similar results (54). They, however, considered the nonadiabatic crossing between spin-orbit excited and ground-state surfaces.

We have examined another class of reactions exhibiting both reactive and nonreactive channels, the collision of halogen atom with alkyl halides (38):

$$CH_3I + I \rightarrow CH_3\cdots I\cdots I^{\ddagger} \rightarrow$$

$$CH_3I + I; \quad CH_3 + I_2.$$

The reaction, initiated in the $(CH_3I)_2$ complex, can either proceed through the inelastic (CH_3I + I) or reactive channel (CH_3 + I_2). The departing CH_3 radical carries away most of the available energy, leaving the iodine atom with only enough energy for inelastic scattering. The lifetime of the collision complex is ≈1.7 ps. Although the reactive channel is expected to be energetically inaccessible, the I_2 product is formed in 500 fs. This observation suggested a four-center reaction mechanism involving cooperative motion of both C–I bonds, a Bodenstein-type reaction.

Other studies of bimolecular reactions in real time have been carried out in the laboratories of Wittig at the University of Southern California (53), McDonald at the University of Illinois (54), and Stephenson at the National Institute of Standards and Technology (55), as well as other laboratories.

Bimolecular Electron-Transfer Reactions

Common to all electron-transfer (ET) reactions is the coupling between ionic and covalent (or ionic and ionic) configurations that establishes a unique transition state. In the entrance channel of a generic bimolecular electron transfer reaction of A + BC (or A* + BC in photoinduced ET), the system converts from being covalent to being ionic in nature through harpooning at long intermolecular separations. In the transition state, the structure $A^+\cdots{}^-BC$ is formed over a range of distances and geometries. In the exit channel, the transition state either adiabatically continues on the harpooning potential to form A^+B^- + C or searches for the covalent channel of AB + C through the ionic–covalent coupling.

We have designed a series of experiments aimed at reaching the transition state directly (26, 27). The fs pulse prepares the transition state $A^+\cdots{}^-BC^{*\ddagger}$ from a well defined ground-state geometry, A···BC. The dynamics is then followed by monitoring the transition state or the reaction products on the fs time scale. For this class of bimolecular reactions, the first study included the complexes of iodine with benzene (Bz) and also with six different methyl-substituted benzenes (26). The Bz···I_2 system is a prototypical electron donor–acceptor complex bearing historic significance dating back to the seminal works by Hildebrand and Mulliken nearly 60 years ago. In the simplest picture, based on Mulliken's theory, the first CT excitation promotes an electron from the highest occupied molecular orbital (HOMO) (π) of benzene to the lowest unoccupied molecular orbital (LUMO) (σ^*) of molecular iodine.

The complex was prepared in supersonic molecular beams under carefully controlled conditions favoring only the 1:1 complex. At $t = 0$, the transition state, $Bz^+\cdots I_2^-$, is reached by fs CT excitation, and the reaction was followed by monitoring both the transition state decay and product iodine atom(s), with time, speed, and angular resolutions, using fs mass spectrometry. Free iodine atoms appear with an apparent rise time of 750 fs, and the initial transition state decays with a time constant of ≈250 fs in a biexponential behavior. By resolving the kinetic energy, the apparent rise of 750 fs was found to be a synthesis of two components with distinct kinetic energies and temporal behaviors: the high-energy component rises in 450 fs, whereas the low-energy component builds up in 1.4 ps. The recoil anisotropy was also measured for the two distributions. From these experiments, the direction of recoil, relative to that of the transition dipole moment, was established, indicating that the molecular structure has iodine tilted, not axial or parallel to the benzene plane as commonly discussed in the literature.

The reaction dynamics and mechanism must involve two channels, one that produces Bz^+I^- + I, and a second neutral pathway, Bz···I + I. The general picture is the following. After fs initiation of the CT, the prepared transition-state wave packet moves on the CT surface and bifurcates near the ionic-neutral region. Some portion of the population continues on the adiabatic, harpoon potential. The remaining, larger portion of the population then in 250 fs switches to the neutral repulsive surface through back electron transfer (from an inner σ orbital of iodine to the π of benzene), leading to a direct I + I dissociation. The uncaged iodine atom dissociates nearly freely and gives rise to the 450-fs high-kinetic-energy component. The caged iodine atom, on the other hand, encounters the donor molecule (benzene) and slowly escapes from its force field with significant loss in translational energy. This one-molecule caging mechanism was later confirmed by a similar experiment on Bz···ICl complex (27). In this case, there is only one iodine atom

facing benzene, and we observed a dominant low-kinetic-energy component.

For larger-solvated-clusters, $(Bz)_n \cdots I_2$, the behavior of releasing iodine atoms on two different time scales was found to be robust, but with changes in time scales. As the size increases, the rise becomes slower, reaching longer than 2 ps; a much slower component gradually grows in with time constants of ≈20–75 ps (26, 49). Using Monte Carlo and molecular dynamics simulation, we found that this effect arises from a fundamental asymmetry in the structure of the clusters (56). The benzenes tend to form mouth-shaped structures around the iodine, or equivalently, the iodine is partially "immiscible" in benzene, causing one of the iodine atoms to be more strongly solvated than the other. The faster component (a few ps) is due to the iodine atom facing away from the cluster, and the much slower component is due to trapping of the other iodine atom by the cluster. This caging dynamics is a probe of structural features of solvation.

In liquids, aromatic$\cdots I_2$ systems have been studied by measuring the transient absorption of the product aromatic$\cdots$I species (57, 58). The rise times were found to be 25 fs followed by 450 fs (57). Although the time scales are also ultrashort, the complexity arises from several processes involved: transient absorption of aromatic$\cdots$I can develop before complete I–I bond breakage and free I atom formation; bulk solvent–solute interactions may result in faster ionic-neutral switching; and the energies of covalent and ionic surfaces may change. It is important to note that, although the results obtained in liquid-solution studies are important in their own rights, a detailed microscopic picture of the dynamics discussed above cannot be obtained in bulk solutions because of the substantial caging and recombination effects by the surrounding solvent molecules.

In addition to these aromatic$\cdots I_2$ complexes, we have also studied other types of complexes in which the donor donates an electron from a nonbonding orbital of a heteroatom to the σ^* orbital of the acceptor I_2 (27). This type of nσ complex is to be distinguished from the aromatic$\cdots I_2$ complexes in which the donating electron comes from the aromatic π orbital. The nσ complexes we have studied included diethylsulfide$\cdots I_2$, *p*-dioxane$\cdots I_2$, and acetone$\cdots I_2$. Results of similar behavior to those of Bz$\cdots I_2$ complex were obtained for all three systems, suggesting that back electron transfer leading to I_2 dissociation is of general nature, and is mechanistically significant.

Acid–Base Proton-Transfer Reactions

Proton transfer is another important elementary process that is omnipresent in chemistry and biology. In the systems we studied, electronic excitation of the acid induces an instantaneous change in its proton affinity, i.e., a pH jump, leading to the transfer of a proton, an acid–base reaction ($AH^*\cdots B \rightarrow A^-\cdots H^+B$). In a simple double-well picture, the initial configuration, $AH^*\cdots B$, is governed by neutral interactions, covalent and hydrogen bonds, whereas the product configuration, $A^-\cdots H^+B$, is mainly ionic in character. The shape of the potential surface, especially in the barrier and product-state regions, is greatly dependent on solvent number and local structure, both statically and dynamically. Vibrational relaxation, intramolecular vibrational redistribution (IVR), and solvent rearrangement (solvation) are also expected to play a role in stabilizing the product configuration. Studies of these reactions in clusters are thus critical for addressing dynamical issues at the microscopic level.

The first system we studied was that of 1-naphthol (1-NpOH) as the acid and ammonia, piperidine, or water as the base solvent, with the number (n) of solvent molecules varying (20–22). Time-resolved fluorescence and ps and fs ionization mass spectrometry were carried out to investigate the dynamics of each cluster. We have examined the cluster size dependence, vibrational energy dependence, isotope effect, and the effect of solvent type (22). The excited state of the bare 1-naphthol molecule was observed to decay exponentially with a time constant of ≈60 ns. Reactive clusters exhibited biexponential decay behavior indicating the occurrence of proton transfer. The fast component (few tens of ps) was ascribed to the reversible proton transfer process, whereas the slow component (few ns) was assigned to the irreversible equilibration of the system after proton transfer (22).

For the ammonia clusters, proton transfer occurs at a critical number of about $n = 3$, whereas for piperidine, $n = 2$. These results suggested that, in finite-sized clusters, the ion-pair complex is formed on the ps time scale and the solvent rearrangement takes place on the nanosecond time scale for further stabilization of the acid–base product state. Comparisons of the rates for 1-NpOH$\cdots(NH_3)_{3,4}$ and 1-NpOD$\cdots(ND_3)_{3,4}$ showed a large isotope effect of ≈3–4. The water clusters exhibited no sign of short time-scale (ps) dynamics for $n = 1$–21, indicating, by analogy, that proton transfer/reorganization is inactive (22). The distinct cluster size thresholds for proton transfer and the variation among different solvents were explained by using a simple model considering the thermodynamics of solvation and Coulombic potential energies for the ion-pair state. It was suggested that the resistance of the water clusters to promote proton transfer may be due to the tendency of water molecules to concentrate near the OH group of 1-NpOH. Thus, there is incomplete solvation of the naphtholate anion, at least for intermediate-sized clusters (59). The reaction time scale, vibrational energy dependence, and deuterium isotope effects are all consistent with a tunneling mechanism (22). The phenol$\cdots(solvent)_n$ system has been extensively studied by Syage (60).

Another system that has been studied in our group is the excited-state double proton transfer in a model base pair, the 7-azaindole (7-AI) pair, containing two hydrogen bonds (29). Since the discovery of the DNA double helix structure by Watson and Crick in 1953, this aspect of tautomerization as a cause of mutation in DNA hydrogen-bonded base pairs has been the subject of numerous studies. There are two possible mechanisms for proton transfer: a stepwise transfer through an intermediate structure, or a direct cooperative transfer to the tautomer structure. Although it is appealing to describe the transfer in solution phase by a simple double well, studies of isolated base pair complexes can shed light on the nature of intramolecular transfer.

In our experiments, the 7-AI pair was produced in a molecular beam and was studied by fs ionization mass spectrometry (29). We resolved a biphasic behavior, suggesting a stepwise mechanism for the isolated pair. The first step occurs in 0.65 ps to form an intermediate, whereas the second step to form the final tautomer takes place in 3.3 ps. We have also studied the vibrational energy dependence and the deuterium isotope effect, and the results were consistent with a two-dimensional tunneling model involving the N–H and N$\cdots$N motions. Because the transfer is faster than IVR (at low vibrational energies), it is reasonable to describe the motion in the N–H$\cdots$N coordinate. The findings were supported by *ab initio* and MD calculations in other laboratories. Independently, the Castleman group, by using the Coulomb explosion technique, has arrested the intermediate (61) and shown that its rise is similar to our time constants, providing further evidence of the two-step mechanism. M. Kasha believes in the concerted mechanism, but as we have discussed elsewhere (62–64), for both elementary systems and those in the condensed phase, trajectories of an exact concerted motion are in the minority of dynamics on multidimensional surfaces.

Hydrated Electrons

Since the first observation of solvated electrons in liquid ammonia in 1864, the nature of excess electrons in liquids has continued to attract much attention. The existence of the solvated electron in liquid water, i.e., the hydrated electron, was confirmed in 1962 by recording its transient absorption spectrum. The hydrated electron is central to a myriad of physical, chemical, and biological processes.

In a simple picture of an electron in a solvent cavity, the description of hydrated electrons is analogous to that of a hydrogen atom, with a ground state of *s*-type and an excited state of *p*-type character. A key issue for understanding electron hydration is knowledge of the time scales involved: the motion of water molecules toward the equilibrium structure and the lifetime of the electron in the different state it occupies. Although these points have been addressed in bulk studies, there remain unanswered questions, especially regarding the microscopic molecular structure and dynamics of hydration. Electrons solvated in finite-sized water clusters provide a unique opportunity for elucidating the influence of microscopic water structure on electron hydration dynamics. In addition, because of the charge of the electron, it is possible to select a particular size of cluster and study its isolated structure and dynamics.

We generated negatively charged water clusters by crossing a continuous electron beam with a jet of water vapor (30). The clusters with sizes up to $n = 35$ were selectively intercepted by fs pulses to promote the electron from the *s*- to the *p*-state. A delayed fs pulse was used to photodetach the electrons that were collected and analyzed with a magnetic-bottle photoelectron spectrometer. The excitation of the hydrated electron initiates the solvent motion toward equilibrium. We followed the subsequent relaxation dynamics by monitoring the evolution of the photoelectron spectrum with kinetic energy resolution (30).

Specifically, we focused our attention on the dynamics in $(H_2O)_n^-$ systems with different solvation cavities, $n = 15$, 20, 25, 30, and 35. By measuring the time dependence of specific regions on the potential energy surface, we resolved a solvation time of ≈300 fs in the *s*-state after internal conversion, for all cluster sizes studied. This time scale is similar to the electron solvation time in bulk water. Such weak size dependence and the similarity between bulk and clusters indicate that the dynamics of the hydration are in large part controlled by the local structure of water molecules in immediate contact with the electron. A much slower relaxation process with size-dependent time constants ranging from 2 to 10 ps was also observed and was attributed to the evaporation of clusters. Together with the experimental work from the groups of Johnson (65) and Neumark (66), these results provide the microscopic time scales involved, and the nature of the state (surface or bulk) in which the electron is being wetted or hydrated. For bulk studies, with and without scavengers, we measured the overall relaxations involved and cautioned about their origin (67).

Barrier-Crossing Reactions

The molecule *trans*-stilbene has long served as a prototype system for the study of photoisomerization and of the influence of solvent on barrier-crossing reactions. Both *trans*-stilbene and *cis*-stilbene undergo ultrafast isomerization by a twist about the central ethylenic bond when excited to their S_1 electronic states, in a process similar to that which occurs in retinal, for example, as a key step in vision. A barrier to isomerization of ≈1,200 cm^{-1} exists in the energy landscape of the isolated *t*-stilbene molecule, as reflected in the excess vibrational energy dependence of the microcanonical isomerization rate, $k(E)$, first measured for a jet-cooled molecular sample in 1982 (ref. 68; for later work on the subject, see refs. 9–11). This barrier is postulated to arise from a curve crossing along the twist coordinate of S_1 with another electronic state (S_n). Extensive time-resolved studies of the isomerization of *t*-stilbene in the isolated molecule and an array of gaseous and condensed phase environments have given a detailed picture of the dependence of the rate on solvent, temperature, and pressure, providing the basis for numerous theoretical treatments. An important observation that has been a stimulus for many of these theoretical investigations is the accelerated rate of isomerization in low-viscosity solutions compared with that predicted from the microcanonical rates of the isolated molecule.

To elucidate the role of microscopic solvation on barrier crossing reactions, we studied the isomerization of isolated *t*-stilbene···solvent clusters (24, 69). The clusters (*t*-stilbene···hexane$_n$, $n = 1$–5, and several isotopic variants thereof, and *t*-stilbene···octane$_n$, $n = 1$, 2) were generated in a seeded molecular beam, and the dynamics associated with clusters of different stoichiometry were independently resolved by means of ionization and mass-selective, time-of-flight detection. By this experimental approach, the effect of limited and specific solvent-solute interactions was investigated in the absence of the statistical interaction that characterizes collisional friction with an external medium.

Three distinct factors that influence isomerization in an isolated molecule and that may be changed by complexation are the reaction potential, the effective inertia for motion in the isomerization coordinate, and the density of states. The solvent vibrational modes and the low-frequency intermolecular cluster modes add a large energy bath to the system. This bath will slow the reaction in an initially cold cluster by inhibiting vibrational energy deposited by the excitation source from reaching the reaction coordinate, an effect which may be referred to as "energy friction," different from "collisional" friction associated with the solvent molecule constituting a physical or inertial impediment to motion along the reaction coordinate (70).

A general property that is immediately evident from our experimental results is the fact that for each solute···solvent$_n$ series, the isomerization rates at equal excess energies well above the isomerization barrier decrease systematically with increasing cluster size (increasing n). In all cases for which the excess energy dependence of the isomerization rate was well determined, it could be accounted for by a consistent application of nonadiabatic statistical theory, with the isomerization barrier and degree of adiabaticity as adjustable parameters. The extracted isomerization barriers of the clusters were found to be lower than that of isolated *t*-stilbene, with the barrier height reduction in *n*-hexane clusters being similar to that derived from solution phase studies (71). The lowering of the isomerization rate, despite the reduced barrier to reaction, is attributed to the increased density of vibrational states in the clusters, or "energy friction," and to a substantial reduction in adiabaticity. The latter effect may be explained by a reduction in the coupling between the S_1 and S_n surfaces, resulting from the perturbation of the transition state by the solvent molecule.

Although the rates in the clusters, at fixed energy, are lower than for isolated *t*-stilbene, thermal rates calculated from these lower cluster $k(E)$ values are nevertheless higher than for isolated *t*-stilbene, due to the role of the higher density of states in the thermal average. However, the calculated cluster thermal rates are still lower than the measured solution-phase rates, indicating that one or more additional factors contribute to an acceleration of the solution-phase isomerization relative to the dynamics measured in the small cluster limit. One such factor examined in a number of previous studies and found to be consistent with the cluster results (69) is an increase in the adiabaticity of the reaction (72) in the liquid environment, reversing the effect deduced for small clusters. In this case, the cause may

be simply a slowing of velocity along the reaction coordinate during passage over the barrier by random collisions with a full shell of surrounding solvent molecules. Such insights into the respective roles of interaction of the reactant with individual solvent molecules and statistical effects of friction associated with the liquid medium as a whole are a primary motivation for the study of these isolated clusters.

Biological Analogues

A different aspect of the subject of molecular complexes is represented by the process of molecular recognition and transport of small ligands by proteins and protein mimics. The natural systems of hemoglobin and myoglobin form reversible complexes with O_2 that are involved in the transport of O_2 in biological systems. "Picket fence" porphyrins represent one of the many synthetic models of these biological systems. These natural and synthetic systems can be studied as complexes, and for them we examined the nature of dative bonding, elementary steps of reactions, and molecular recognition.

Picket-Fence Porphyrins. Femtosecond transient absorption measurements were made of four-coordinate picket fence cobalt(II) porphyrin in benzene at room temperature, its five-coordinate 1-methylimidazole (1-MeIm) adduct, and the six-coordinate O_2 complex of the 1-MeIm adduct. The transient behavior for the two O_2-free porphyrins was very similar to that for cobalt(II) tetraphenylporphyrin. However, a dramatic change in the transient absorption was observed when the porphyrin was oxygenated. These observations indicated the release of the bound O_2 from the active binding site with a total reaction time of 1.9 ± 0.4 ps (39).

The dative bonding, similar to that of Bz and I_2, of cobalt to O_2 critically depends on the interaction of the d_{z^2} orbital on Co with the π^* orbital on O_2 (through a σ-type interaction), and on the back-bonding from the metal d-π orbitals to O_2. The non-collinear configuration enhances the σ-bonding, and, because the Co d_{z^2} electron is engaged, the oxidation state of Co approaches +3. After fs excitation and an initial ultrafast relaxation within the porphyrin system (200 fs), charge transfer from the porphyrin-based π system to the base–metal–O_2 system restores an electron to the cobalt d_{z^2} orbital and weakens the metal–O_2 bond. Reverse charge-transfer and release of the O_2 can then occur in concert to produce the free porphyrin in its ground state with a total reaction time of 2 ps.

The fact that, after the oxygen release, the transient absorbance does not recover appreciably on the nanosecond time scale shows that the extent of geminate rebinding of O_2 is small. On much longer time scales, the system does return to equilibrium, with the thermal binding dynamics determined by the global energy landscape for the recognition process. By extending the time window of the transient absorption measurements to the microsecond range using an electronic delay of the probe pulse, the total rebinding dynamics could be followed, and a study of their dependence on temperature and oxygen concentration was carried out (40). The extracted rate constants, from single-exponential decays, vary linearly with oxygen concentration. This behavior is consistent with a two-state kinetic model with one reversible step of bimolecular association (k_{on}) and unimolecular dissociation (k_{off}), under a pseudo-first-order reaction condition, i.e., when oxygen concentration is much greater than that of the porphyrin molecule. However, when analyzed according to this model, the data yield a k_{on} that is 30–60 times smaller than that calculated from standard Smoluchowski theory for a diffusion-controlled reaction, and with a temperature dependence that also fails to conform to the theoretically expected trend.

To address these inconsistencies, we considered a different model that includes two reversible steps and a reaction intermediate. In this model, the two processes are represented by

$$P + O_2 \rightleftharpoons P\cdots O_2 \rightleftharpoons P\text{–}O_2,$$

where P is the picket fence porphyrin and $P\cdots O_2$ stands for the intermediate complex, in which the O_2 is associated with the porphyrin structure but the strong ligand–metal bond has not been formed. This two-step model provides a physical basis for the discrepancy between k_{on} and the Smoluchowski diffusion-controlled rate constant by showing that most of the diffusion-controlled encounters which lead to the formation of the intermediate do not result in a final bound state. The apparently anomalous weak temperature dependence of k_{on} follows naturally.

In conclusion, excitation of the O_2 complex of the picket fence porphyrin within the Q-band leads to ultrafast (2 ps) ejection of O_2, which is a reflection of the influence of charge redistribution within the complex on the O_2–Co dative bond. Femtosecond excitation and ultrafast entry to the transition state allowed us to study the direct evolution to products and to dissect the elementary steps. The rates involved in the *thermal* bimolecular recognition and their temperature and concentration dependencies were determined, and consistency of the thermodynamics, kinetics, and dynamics was achieved via a two-step model, with reversibility of both steps, which describes the recognition of the macromolecule, most probably nonselectively, and the selective reaction inside the structure.

Myoglobin (Mb). In our study of Mb, a combination of protein engineering (mutagenesis) and ultrafast spectroscopy was used to investigate the relationship of structure and function by measuring the effect on O_2 rebinding dynamics produced by changes in specific protein residues located near the heme iron center. Complexes of Mb with O_2 were studied at room temperature. In addition to the WT protein, two mutants were chosen, in one of which there exists a structural blockage to escape of O_2 from the distal cavity. These mutations had previously been demonstrated to affect the ligand nanosecond geminate rebinding as well as the overall bimolecular rebinding kinetics. On the ultrashort time scale, a 5- to 6-ps geminate recombination of O_2 with WT Mb had been reported, but this ultrafast recombination process, the ultimate step in formation of the protein–ligand bond, had not been resolved in the mutants. Our fs-resolved transient absorption study, with a time window extending up to 10 ns, allowed the response to photolysis of all three systems to be fully characterized, revealing that, although behaviors differ distinctly among mutants on long time scales, on the ultrafast time scale they are essentially the same.

Our observation of an unchanging rate and fraction for ps rebinding contradicts the predictions of MD simulations (73) for the mutant effect under the assumption of a homogeneous sample. To account for the discrepancy, we proposed that the ultrafast primary step follows the dynamics of the "bifurcation model," which was found to be significant in ultrafast chemical and biological reactions (ref. 10 and references therein). In this case, because of protein conformations with low free energy barriers to recombination, a "directed population" will rebind within the first few ps, whereas an "undirected population" will be in conformations capable of recombination following thermal and intramolecular motions on a longer time scale. Because the escape fraction is determined by the conformational bifurcation rather than the competition between forward and backward rates, as long as recombination is highly favored in the directed population of the WT, the obstruction of the forward path in the mutant will have little effect on the ultrafast time scale, as we observed.

This bifurcation picture raises an important point about the nature of the energy landscape and trajectory of motions. On the fs to ps time scale, the protein is es-

sentially a frozen matrix, and only small and local conformational changes (lower level of conformational tiers) may be involved. The directed geminate recombination takes place on one family of conformations that is adapted to ensure efficient reformation of the metal–ligand bond on a static or minimally fluctuating landscape, and we observe no change of rates or fractions with mutation. Larger and global motions in the protein occur at longer time. Those motions involve transitions of higher tiers of conformational structures. On such time scales, the trajectories visit a large phase space and the landscape fluctuations play a role, including interconversion between directed and undirected conformations. In such a situation, a mutant effect on the protein global fluctuation will alter the rebinding dynamics.

In summary, the lack of a pronounced mutation effect on the initial rebinding shows that this process is kinetically isolated from the distal pocket environment through which the ligand moves on the nanosecond time scale. The bifurcation that allows this isolation is understood in terms of a distribution of conformational structures, with one set of conformations leading to directed O_2–Fe bond formation without sampling a large phase space. The fact that mutation causes a drastic effect on rebinding dynamics on the time scale of protein global fluctuation is consistent with this concept of directed populations. The existence of conformations optimized for directed bonding in MbO_2 should be important for an efficient biological function (10).

Conclusion

This short review highlighted our effort at Caltech in the study of the dynamics of clusters, from elementary systems to the complexes of biological structures. Throughout these studies, our focus was on probing the microscopic dynamics, and our goal was in bridging the isolated system behavior to that of the bulk. The scope of phenomena is rich because of the fundamental nature of clusters, their controllable finite size, their elucidation of the critical role of stepwise solvation, and their use as precursors for reactions. Many of the concepts derived from the study of elementary chemical systems were applied in the exploration of the dynamics of biomolecular complexes.

From such studies a number of new concepts have emerged, including those describing the mechanism of fragment caging in solvent shells (hard sphere interaction vs. vibrational energy loss), local sphere solvation (as opposed to continuum model solvation), ultrafast back electron transfer (which describes phenomena of chemical and biological nature), critical solvent-size effect in proton and electron transfer reactions, and the determining role of collision complex lifetimes in controlling the outcome of reactions. These concepts are fundamental to the description of phenomena on the nanometer scale, because they are the result of studies on such a scale, with size selection, and not in the bulk phases. For biological dynamics and function these concepts are also relevant.

One of the most significant findings in ultrafast dynamics of complex systems is the ability of such systems to direct energy through electronic and nuclear couplings to enhance the efficiency and useful work. This became evident in early studies of femtochemistry and similarly in femtobiology (10). For high efficiency, chemical and biological systems direct the energy by limiting the phase space to a few coordinates, and this avoids dissipation or wasting of energy. As discussed elsewhere (10), this directivity is greatly aided by the robustness of the original vibrational coherence. From the visual pigment rhodopsin to heme ligated myoglobin (74), these directed motions are important to the function. In general, one must ask about the relevance of photon-driven systems to those functioning by thermal motions. Many systems use the light to reach the product ground state with high efficiency. Thus, although subsequent events may occur on longer time scales, it is crucial to understand the primary process, and thermal reactions may use the same pathway but with much lower efficacy.

Studies of isolated systems provide an additional dimension in our understanding of the role of complex environments, such as proteins, in the process of molecular evolution. In a recent study from this laboratory (75), we were able to probe the dynamics of the isolated negative anion chromophore of PYP (photoactive yellow protein) and compare with its dynamics in the protein environment. Remarkably, the role of the protein is to reduce the phase space and prepare the ground state in <1 ps, and without creating the radical species that is detected in the isolated chromophore. This is achieved by using a few nuclear motions (bond rotation/twisting) and a conical intersection. Such studies, and those with stepwise hydration, allow us to uncover the nature of the forces involved and purpose of biological complexity.

The success in the studies of dynamics has also triggered the determination of isolated cluster structures using rotational coherence spectroscopy developed in this laboratory (76, 77). Numerous cluster structures have been determined (for a review, see refs. 78 and 79), but what remains undetermined are the transient structures involved in the dynamics. This challenge of structural dynamics represents our next frontier in the world of clusters and biological systems (80).

P.-Y.C. thanks the National Science Council of Taiwan for sabbatical support in 2005 at the California Institute of Technology. This work was supported by a grant from the National Science Foundation.

1. Dermota, T. E., Zhong, Q. & Castleman, A. W., Jr. (2004) *Chem. Rev.* **104,** 1861–1886.
2. Castleman, A. W., Jr., & Bowen, K. H., Jr. (1996) *J. Phys. Chem.* **100,** 12911–12944.
3. Brutschy, B. & Hobza, P., eds. (2000) *Chem. Rev.* **100,** 3861–4264.
4. Bernstein, E. R., ed. (1996) *Chemical Reactions in Clusters* (Oxford Univ. Press, New York).
5. Syage, J. A. & Zewail, A. H. (1998) in *Advances in Molecular Vibrations and Collision Dynamics*, eds. Bowman, J. M. & Bačić, Z. (JAI Press, Stamford, CT), Vol. 3, pp. 1–60.
6. Felker, P. M. & Zewail, A. H. (1983) *J. Chem. Phys.* **78,** 5266–5268.
7. Felker, P. M. & Zewail, A. H. (1983) *Chem. Phys. Lett.* **94,** 448–453.
8. Felker, P. M. & Zewail, A. H. (1983) *Chem. Phys. Lett.* **94,** 454–460.
9. Zewail, A. H. (1994) *Femtochemistry-Ultrafast Dynamics of the Chemical Bond* (World Scientific, Singapore).
10. Zewail, A. H. (2000) in *Les Prix Nobel: The Nobel Prizes 1999*, ed. Frängsmyr, T. (Almquist & Wiksell, Stockholm), pp. 103–203.
11. Zewail, A. H. (1983) *Faraday Discuss.* **75,** 315–330.
12. Phillips, D. (2003) *100 Years of Physical Chemistry, Royal Society of Chemistry* (Black Bear Press, Cambridge, U.K.), pp. 105–106.
13. Semmes, D. H., Baskin, J. S. & Zewail, A. H. (1987) *J. Am. Chem. Soc.* **109,** 4104–4106.
14. Semmes, D. H., Baskin, J. S. & Zewail, A. H. (1990) *J. Chem. Phys.* **92,** 3359–3376.
15. Breen, J. J., Willberg, D. M., Gutmann, M. & Zewail, A. H. (1990) *J. Chem. Phys.* **93,** 9180–9184.
16. Willberg, D. M., Gutmann, M., Breen, J. J. & Zewail, A. H. (1992) *J. Chem. Phys.* **96,** 198–212.
17. Gutmann, M., Willberg, D. M. & Zewail, A. H. (1992) *J. Chem. Phys.* **97,** 8037–8047.
18. Gutmann, M., Willberg, D. M. & Zewail, A. H. (1992) *J. Chem. Phys.* **97,** 8048–8059.
19. Wan, C., Gupta, M., Baskin, J. S., Kim, Z. H. & Zewail, A. H. (1997) *J. Chem. Phys.* **106,** 4353–4356.
20. Breen, J. J., Peng, L. W., Willberg, D. M., Heikal, A., Cong, P. & Zewail, A. H. (1990) *J. Chem. Phys.* **92,** 805–807.
21. Kim, S. K., Wang, J. K. & Zewail, A. H. (1994) *Chem. Phys. Lett.* **228,** 369–378.
22. Kim, S. K., Breen, J. J., Willberg, D. M., Peng, L. W., Heikal, A., Syage, J. A. & Zewail, A. H. (1995) *J. Phys. Chem.* **99,** 7421–7435.
23. Lienau, C., Heikal, A. A. & Zewail, A. H. (1993) *Chem. Phys.* **175,** 171–191.
24. Heikal, A. A., Chong, S. H., Baskin, J. S. & Zewail, A. H. (1995) *Chem. Phys. Lett.* **242,** 380–389.
25. Cheng, P. Y., Zhong, D. & Zewail, A. H. (1995) *J. Chem. Phys.* **103,** 5153–5156.
26. Cheng, P. Y., Zhong, D. & Zewail, A. H. (1996) *J. Chem. Phys.* **105,** 6216–6248.
27. Zhong, D. P., Bernhardt, T. M. & Zewail, A. H. (1999) *J. Phys. Chem. A* **103,** 10093–10117.

28. Peng, L. W., Dantus, M., Zewail, A. H., Kemnitz, K., Hicks, J. M. & Eisenthal, K. B. (1987) *J. Phys. Chem.* **91,** 6162–6167.
29. Douhal, A., Kim, S. K. & Zewail, A. H. (1995) *Nature* **378,** 260–263.
30. Paik, D. H., Lee, I. R., Yang, D. S., Baskin, J. S. & Zewail, A. H. (2004) *Science* **306,** 672–675.
31. Paik, D. H., Bernhardt, T. M., Kim, N. J. & Zewail, A. H. (2001) *J. Chem. Phys.* **115,** 612–616.
32. Paik, D. H., Kim, N. J. & Zewail, A. H. (2003) *J. Chem. Phys.* **118,** 6923–6929.
33. Kim, N. J., Paik, D. H. & Zewail, A. H. (2003) *J. Chem. Phys.* **118,** 6930–6940.
34. Scherer, N. F., Khundkar, L. R., Bernstein, R. B. & Zewail, A. H. (1987) *J. Chem. Phys.* **87,** 1451–1453.
35. Scherer, N. F., Sipes, C., Bernstein, R. B. & Zewail, A. H. (1990) *J. Chem. Phys.* **92,** 5239–5259.
36. Gruebele, M., Sims, I. R., Potter, E. D. & Zewail, A. H. (1991) *J. Chem. Phys.* **95,** 7763–7766.
37. Sims, I. R., Gruebele, M., Potter, E. D. & Zewail, A. H. (1992) *J. Chem. Phys.* **97,** 4127–4148.
38. Zhong, D. P., Cheng, P. Y. & Zewail, A. H. (1996) *J. Chem. Phys.* **105,** 7864–7867.
39. Steiger, B., Baskin, J. S., Anson, F. C. & Zewail, A. H. (2000) *Angew. Chem. Int. Ed.* **39,** 257–260.
40. Zou, S. Z., Baskin, J. S. & Zewail, A. H. (2002) *Proc. Natl. Acad. Sci. USA* **99,** 9625–9630.
41. Wang, Y., Baskin, J. S., Xia, T. & Zewail, A. H. (2004) *Proc. Natl. Acad. Sci. USA* **101,** 18000–18005.
42. Knee, J. L., Khundkar, L. R. & Zewail, A. H. (1985) *J. Chem. Phys.* **82,** 4715–4716.
43. Knee, J. L., Khundkar, L. R. & Zewail, A. H. (1987) *J. Chem. Phys.* **87,** 115–127.
44. Heikal, A., Banares, L., Semmes, D. H. & Zewail, A. H. (1991) *Chem. Phys.* **156,** 231–250.
45. Liu, Q. L., Wang, J. K. & Zewail, A. H. (1993) *Nature* **364,** 427–430.
46. Wang, J. K., Liu, Q. L. & Zewail, A. H. (1995) *J. Phys. Chem.* **99,** 11309–11320.
47. Liu, Q. L., Wang, J. K. & Zewail, A. H. (1995) *J. Phys. Chem.* **99,** 11321–11332.
48. Cheng, P. Y., Zhong, D. & Zewail, A. H. (1995) *J. Phys. Chem.* **99,** 15733–15737.
49. Cheng, P. Y., Zhong, D. & Zewail, A. H. (1995) *Chem. Phys. Lett.* **242,** 369–379.
50. Douhal, A., Zhong, D. & Zewail, A. H. (2002) in *Femtochemistry and Femtobiology*, eds. Douhal, A. & Santamaria, J. (World Scientific, Singapore), pp. 731–741.
51. Zewail, A. H. (1988) *Science* **242,** 1645.
52. Wittig, C. & Zewail, A. H. (1996) in *Chemical Reactions in Clusters*, ed. Bernstein, E. R. (Oxford Univ. Press, New York), pp. 64–99.
53. Ionov, S. I., Brucker, G. A., Jaques, C., Valachovic, L. & Wittig, C. (1993) *J. Chem. Phys.* **99,** 6553–6561.
54. Tuchler, M. F., Wright, S. & McDonald, J. D. (1997) *J. Chem. Phys.* **106,** 2634–2645.
55. Miller, C. C., van Zee, R. D. & Stephenson, J. C. (2001) *J. Chem. Phys.* **114,** 1214–1232.
56. Su, J. T. & Zewail, A. H. (1998) *J. Phys. Chem. A* **102,** 4082–4099.
57. Lenderink, E., Duppen, K. & Wiersma, D. A. (1993) *Chem. Phys. Lett.* **211,** 503–510.
58. Pullen, S., Walker, L. A. & Sension, R. J. (1995) *J. Chem. Phys.* **103,** 7877–7886.
59. Knochenmuss, R. & Leutwyler, S. (1989) *J. Chem. Phys.* **91,** 1268–1278.
60. Syage, J. A. (1995) in *Femtosecond Chemistry*, eds. Manz, J. & Wöste, L. (VCH, New York), Vol. 2, pp. 475–498.
61. Folmer, D. E., Wisniewski, E. S., Hurley, S. M. & Castleman, A. W., Jr. (1999) *Proc. Natl. Acad. Sci. USA* **96,** 12980–12986.
62. Fiebig, T., Chachisvilis, M., Manger, M., Zewail, A. H., Douhal, A., Garcia-Ochoa, I. & Ayuso, A. D. H. (1999) *J. Phys. Chem. A* **103,** 7419–7431.
63. Zhong, D. P. & Zewail, A. H. (1998) *J. Phys. Chem. A* **102,** 4031–4058.
64. Møller, K. B. & Zewail, A. H. (1998) *Chem. Phys. Lett.* **295,** 1–10.
65. Hammer, N. I., Shin, J. W., Headrick, J. M., Diken, E. G., Roscioli, J. R., Weddle, G. H. & Johnson, M. A. (2004) *Science* **306,** 675–679.
66. Bragg, A. E., Verlet, J. R. R., Kammrath, A., Cheshnovsky, O. & Neumark, D. M. (2004) *Science* **306,** 669–671.
67. Lu, Q. B., Baskin, J. S. & Zewail, A. H. (2004) *J. Phys. Chem. B* **108,** 10509–10514.
68. Syage, J. A., Lambert, W. R., Felker, P. M., Zewail, A. H. & Hochstrasser, R. M. (1982) *Chem. Phys. Lett.* **88,** 266–270.
69. Chong, S. H. (2001) Ph.D. thesis (California Institute of Technology, Pasadena).
70. Fleming, G. R. & Hanggi, P., eds. (1993) *Activated Barrier Crossing* (World Scientific, Singapore).
71. Schroeder, J., Schwarzer, D., Troe, J. & Voss, F. (1990) *J. Chem. Phys.* **93,** 2393–2404.
72. Felker, P. M. & Zewail, A. H. (1985) *J. Phys. Chem.* **89,** 5402–5411.
73. Quillin, M. L., Li, T. S., Olson, J. S., Phillips, G. N., Dou, Y., Ikedasaito, M., Regan, R., Carlson, M., Gibson, Q. H., Li, H. Y. & Elber, R. (1995) *J. Mol. Biol.* **245,** 416–436.
74. Champion, P. M. (2005) *Science* **310,** 980–982.
75. Lee, I.-R., Lee, W. & Zewail, A. H. (2006) *Proc. Natl. Acad. Sci. USA* **103,** 258–262.
76. Felker, P. M. & Zewail, A. H. (1987) *J. Chem. Phys.* **86,** 2460–2482.
77. Baskin, J. S., Felker, P. M. & Zewail, A. H. (1987) *J. Chem. Phys.* **86,** 2483–2499.
78. Felker, P. M. (1992) *J. Phys. Chem.* **96,** 7844–7857.
79. Felker, P. M. & Zewail, A. H. (1995) in *Femtosecond Chemistry*, eds. Manz, J. & Wöste, L. (VCH, New York), Vol. 1, pp. 193–260.
80. Zewail, A. H. (2005) *Philos. Trans. R. Soc. London A* **363,** 315–329.